de Bono, J., McDowell, G. and Wanatowski, D. (2012) ***Géotechnique Letters* 2**, 199–203, http://dx.doi.org/10.1680/geolett.12.00040

Discrete element modelling of a flexible membrane for triaxial testing of granular material at high pressures

J. DE BONO*, G. MCDOWELL* and D. WANATOWSKI*

The discrete element method (DEM) has been used to simulate triaxial tests on a bonded material at high pressures. A key feature of the model is the use of a flexible membrane that allows the correct volumetric deformation and the true failure mode to develop while applying constant confining pressure to the triaxial sample. The correct pattern of behaviour has been observed across a wide range of confining pressures, with both shear planes and barrelling failure being observed. The radial pressure applied by the membrane remains constant after large strains and deformation.

KEYWORDS: deformation; discrete-element modelling; failure; laboratory tests; numerical modelling; strain localisation

INTRODUCTION

The high-pressure triaxial apparatus has the capacity of applying confining pressures in excess of 64 MPa. The apparatus features the use of flexible membranes, which often vary in thickness according to the confining pressure. Although membrane effects have been acknowledged (Henkel & Gilbert, 1952) they still allow free deformation of the specimen and permit the natural failure mode to develop.

Although a large proportion of numerical work has been in two dimensions (e.g. Utili & Nova, 2008), the widespread availability of the discrete element method (DEM) and advances in computing power have enabled triaxial tests to start to be modelled in three dimensions. Many researchers have simulated true triaxial tests; that is, a cubical sample within flat rigid boundaries (e.g. Sitharam *et al.*, 2002; Belheine *et al.*, 2009; Salot *et al.*, 2009).

For the purposes of simulating accurate laboratory conditions, it is essential that any membrane allows the correct confining pressure to be applied while allowing free deformation. The importance of flexible membranes has been highlighted in recent years. In two dimensions, biaxial tests with flexible membranes have been modelled by researchers such as Iwashita & Oda (1998) and Wang & Leung (2008). In three dimensions, authors such as Cheung & O'Sullivan (2008) and O'Sullivan & Cui (2009) have simulated the effects of confining pressure by applying forces directly to the sample and allowing it to deform freely. However, it is unclear how accurately they accounted for the change in surface area of the sample. They projected the coordinates of the membrane particles to a rectangular plane using Voronoi cells to obtain the corresponding area of each particle. Although effective, this method assumes that the membrane remains cylindrical, but this is not true for a triaxial test with flexible boundaries. Their applied forces were directed towards the centre of the specimen rather than normal to the specimen surface, and their method did not give consideration to the vertical component of confining pressure. Wang & Tonon (2009) simulated the effects of confining pressure in a similar approach at conventional pressures. A disadvantage of solely modelling the effects of confining pressure and not the actual membrane is that it does not leave scope for investigating the role played by the membrane and how its properties affect the behaviour. Nonetheless, these works highlight the important role of flexible boundaries and demonstrate how rigid boundaries inhibit localisation, causing significant non-uniformities in the stresses along the boundary.

Manuscript received 8 June 2012; first decision 6 August 2012; accepted 8 October 2012.
Published online at www.geotechniqueletters.com on 5 November 2012.
*University of Nottingham, Nottingham, UK

DISCRETE ELEMENT MODEL OF A FLEXIBLE MEMBRANE

The software used in this study was PFC3D (Itasca, 2005). The membrane developed consists of a cylindrical array of bonded particles encasing the lateral boundary of the specimen, with discrete forces applied to each particle to give the effect of confining pressure. The membrane particles are hexagonally arranged; the identity of each membrane particle is known, allowing their properties to be retrieved and manipulated easily. It is important that the membrane particles are small enough to prevent penetration of the specimen particles through the membrane. However, their size impacts the calculation time; with this in mind, the membrane particles are generated 33% smaller than the smallest sample particle.

The membrane particles are bonded using 'contact bonds' (Itasca, 2005) that transmit no moments, ensuring membrane flexibility. The bonds are defined by shear and normal tensile strengths, set high enough that the membrane does not split.

Considering the membrane as a series of individual rows allows the vertical surface area to be calculated. Each row consists of a series of particles connected in a loop. The vertical position of a given row is obtained by averaging the z-coordinates of the component particles and the row thickness is approximated by interpolation between the position of that row and adjacent rows (Fig. 1), although all rows have equal thickness initially. The length of each row is obtained by summing the distance between each row particle, obtained from their coordinates. This enables the vertical surface area of the row to be determined; summing for all rows gives the total vertical membrane surface area. Repeating this process, but considering the area enclosed by a polygon (created by the membrane particles) instead of the length gives the volume (Fig. 2).

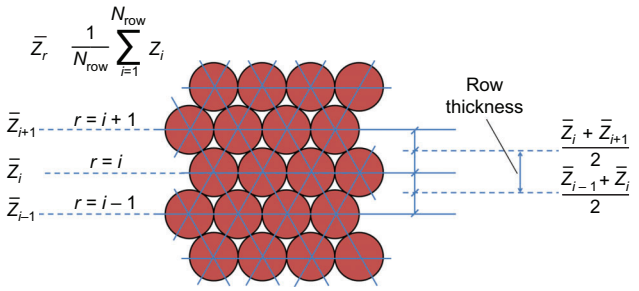

Fig. 1. Detail showing the thickness of row i (consisting of N_{row} number of particles)

For a row of membrane particles, the total horizontal force is the product of the confining pressure and vertical surface area; this force is distributed equally to all the particles in the row. This ensures that the confining pressure is applied evenly to the specimen, regardless of significant changes in shape, and avoids complex calculations used by authors such as Cheung & O'Sullivan (2008). Each discrete horizontal particle force is applied in a direction normal to the membrane surface (i.e. bisecting the line joining two adjacent spheres).

The vertical component of force necessary to give the true confining pressure has little effect on the results until large strains; however, it can be calculated and applied in a similar manner. If the cross-sectional area enclosed by a row of membrane particles is considered along with that for the row above and the row below, this gives a measurement of the local shape of the membrane and the vertical component of confining pressure can then easily be inferred. For example, initially, the horizontal area enclosed by every row of membrane particles will be approximately 0·002 m^2 – the cross-sectional area of the sample before deformation. Because each row has the same horizontal area, this implies no vertical component of confining pressure. After deformation, considering the cross-sectional area of a given row, if the corresponding area of the row above is larger and the row below has a smaller area, this implies an upwards component of force which can be estimated from the disparity in area. The membrane extends beyond the platens by 20%, and the top and bottom loops of particles are fixed to simulate the effects of O-rings (Fig. 3).

MEMBRANE PROPERTIES FOR HIGH PRESSURES

Due to the standard contact model considering stiffnesses to act in series between two interacting objects, it is not possible to calibrate the numerical membrane with laboratory conditions. If the membrane particle normal stiffness (used in tension as well as compression when bonds are used) is adjusted so that the membrane has a realistic 'elastic extension modulus' (Henkel & Gilbert, 1952), excessive overlap occurs between the membrane and the sample when subjected to high confining pressures. The membrane particles completely enter the specimen, disappearing, as shown in Fig. 4(a). Using an artificially high

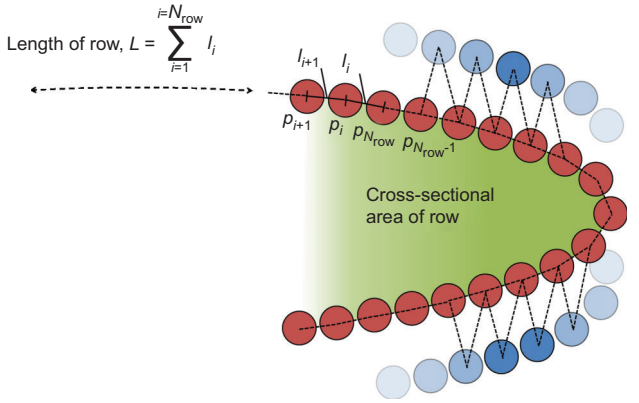

Fig. 2. Schematic diagram illustrating the length and cross-sectional area of a given row of membrane particles

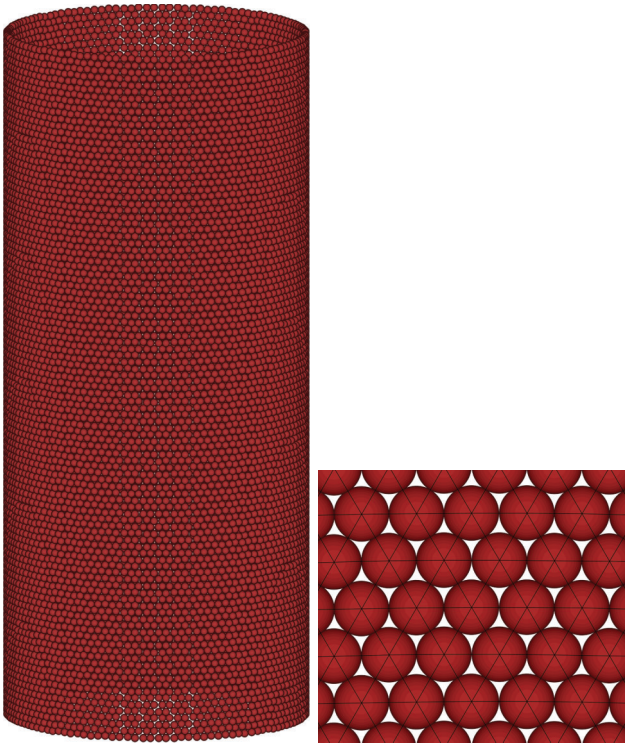

Fig. 3. Numerical membrane consisting of bonded particles

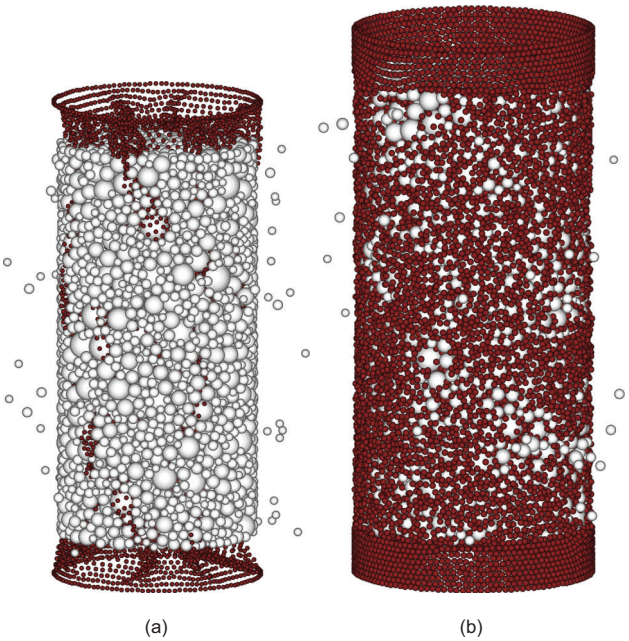

Fig. 4. Failure of the membrane: (a) low particle stiffness causing excessive overlap; (b) membrane particles not staying correctly aligned

Table 1. Membrane properties

Number of particles	11979
Friction coefficient	0·0
Normal and shear stiffness: N/m	$0{\cdot}6 \times 10^6$
Density: kg/m^3	1000
Particle size: mm	0·67
Initial surface area: m^2	0·02

stiffness to prevent this leads to unwanted hoop tension being induced when the specimen expands.

Additionally, the contact normal stiffness is important for particle interaction within the membrane; if the particles are given a high compressive stiffness and low tensile stiffness (user-defined contact model), the particles do not stay aligned. Because of the high pressures, the discrete forces applied to the membrane particles are large enough to render the resistance to tensile displacement between bonded particles negligible; the membrane particles slide apart and behave as if unbonded, as demonstrated in Fig. 4(b).

To avoid a complex user-defined contact model, the particles are given artificially high stiffnesses, with a system in place to adjust the radii of certain membrane particles, relieving the unwanted hoop tension. As the specimen begins to deform, the material typically expands; as the membrane stretches, rows of membrane particles will cover an increased length, accommodated by tensile displacement between the bonded membrane particles. For each row, the mean displacement between neighbouring particles is monitored and if this exceeds 1% of the particle radius, then all the particles in the row are expanded, alleviating the associated forces and avoiding unwanted pressure. The value of 1% means the radii are only expanded by 0·5% at a time, ensuring a gradual process with no sudden overlaps.

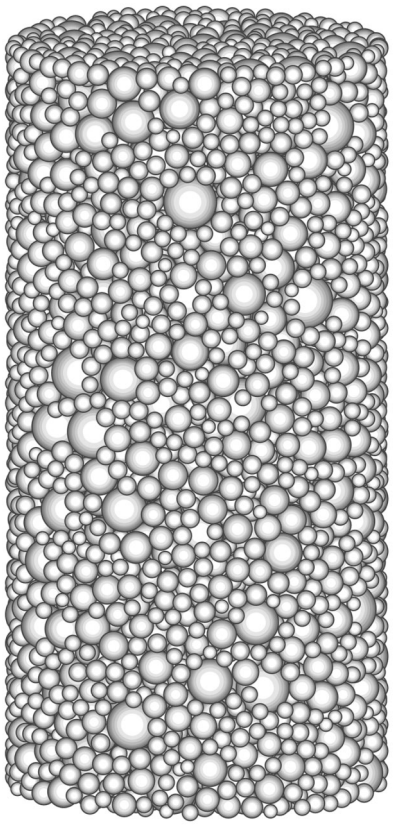

Fig. 5. Numerical specimen, consisting of approximately 7000 particles

Table 2. Sample properties

Sample size: mm	50×100
Number of particles	6759
Friction coefficient	0·5
Normal and shear stiffness: N/m	10×10^6
Density: kg/m^3	2650
Coefficient of uniformity	2·0
Minimum particle diameter: mm	2·00
Median particle size, d_{50}: mm	4·00
Initial void ratio	0·55
Contact model	Linear springs (default)
Damping coefficient	0·7 (default value)

Any value of stiffness above a threshold proportional to the confining pressure can be attributed to membrane particles to prevent them entering the sample. This value can be determined empirically or analytically. For the membrane described in Table 1 and a confining pressure 12 MPa, the minimum required value of stiffness is 0·6 MN/m, which is sufficient to prevent membrane particles sliding apart from one another. Lower values cause the membrane to fail at high strains, while higher values have no effect on the results.

The minor principal stresses are checked using 'measurement spheres' (a function of the software) to ensure that the confining pressure is being applied correctly. Several are used, throughout the height of the specimen, as large as possible without protruding outside the sample. Using a sample (Fig. 5) described by the properties given in Table 2, the membrane's ability to maintain a constant pressure can be demonstrated. The results of two simulations sheared under a confining pressure of 1 MPa are shown in Fig. 6. Both have the same membrane (Table 1); one alleviates hoop tension by the method described, while the other allows hoop tension to be induced. The simulation that alleviates hoop tension by expanding particles ensures a constant minor principal stress; the alternative simulation displays an increasing value, with the rate of increase determined by the membrane particle stiffness. This effect is also visible in the higher value of deviatoric stress. The minor principal stresses were checked for all simulations and in any case never deviated more than 5% from the applied pressure.

For the simulation with constant confining pressure (i.e. alleviating additional hoop tension), increasing the membrane particle stiffness further has a negligible effect on the results. Increasing the membrane particle size reduces the number of contacts between the membrane and the specimen and, if large enough, can lead to specimen particles

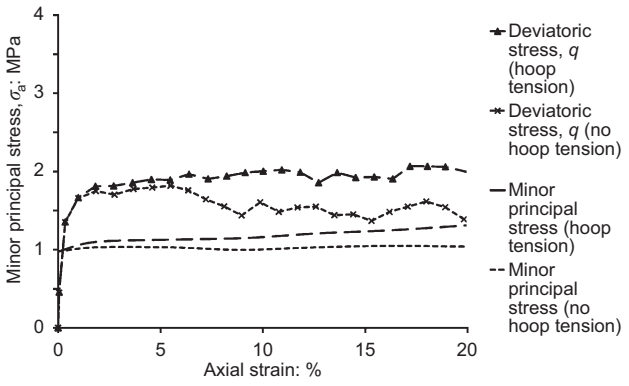

Fig. 6. Minor principal stress and deviatoric stress versus axial strain for unbonded samples sheared at 1 MPa confining pressure

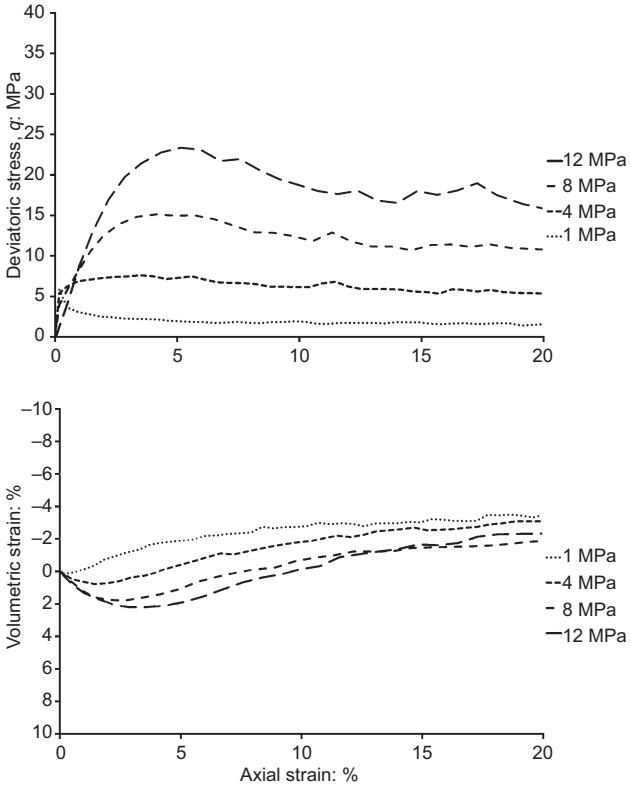

Fig. 7. Triaxial response of bonded material sheared across a range of confining pressures (negative volumetric strain represents dilation)

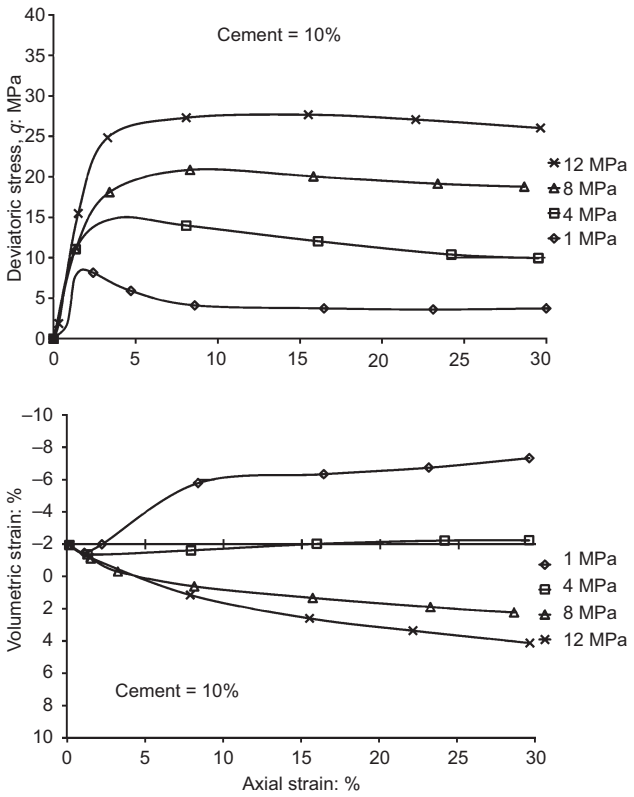

Fig. 8. Triaxial response of cemented sand across a range of confining pressures (Marri *et al.*, 2012)

penetrating the membrane. Giving the membrane particles friction leads to a slight increase in peak stress, although further work is needed to fully clarify the role membrane friction plays in laboratory tests.

FAILURE BEHAVIOUR

A series of simulations featuring a bonded granular material representing cemented sand (used solely to demonstrate brittle deformation) was conducted across a range of confining pressures. Much experimental work has been conducted on cemented sand (Coop & Atkinson, 1993; Schnaid *et al.*, 2001; Asghari *et al.*, 2003; Haeri *et al.*, 2004; Marri *et al.*, 2012) and failure modes have been categorised: brittle failure/shear planes for cemented samples and barrelling failure for equivalent uncemented samples. An increase in confining pressure suppresses the effects of cementation and causes a transition from brittle to ductile behaviour.

The sample particles were bonded using 'parallel bonds' (a cylindrical piece of material between two particles), as used in previous studies (e.g. Potyondy & Cundall, 2004; Wang & Leung, 2008). The bonds are defined by normal and shear stiffness (stress/displacement), normal and shear strength (stress) and size. All bonds have the same size (radius 1 mm). Because this study is not concerned with calibration against physical tests, parallel bond stiffnesses have been defined to give values equal to the particle stiffnesses (force/displacement). The bond strength has been defined so as to give equivalent contact bond strengths of 50 N. The same numerical sample is used, representing Portaway sand (Marri *et al.*, 2012). Parallel bonds representing the cementation were installed at existing contacts between particles before the sample was subjected to confinement. Confining pressure was applied to the specimen, after which the top platen was accelerated over 100 000 timesteps to a velocity of 0·05 m/s.

The use of bonds causes a peak deviatoric stress to appear and increases the maximum stress; varying the magnitude of the bond strength changes the maximum stress and prominence of the peak. Figure 7 shows the triaxial results for the same bonded material sheared at confining pressures of 1, 4, 8 and 12 MPa. Increasing the

Fig. 9. Sheared cemented samples: (a) 1 MPa confining pressure with visible shear planes; (b) 12 MPa confining pressure (Marri *et al.* 2012)

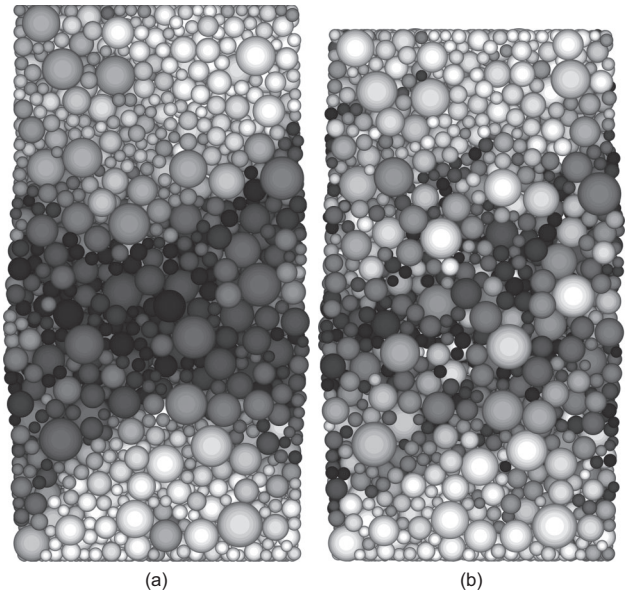

Fig. 10. Particle rotation at maximum rate of dilation for confining pressure of (a) 1 MPa and (b) 12 MPa. Dark grey indicates particles that have undergone the most rotation; white denotes the least rotation

confining pressure leads to a higher maximum deviatoric stress, comparable to the experimental data shown in Fig. 8 (Marri *et al.*, 2012). The strain associated with the maximum stress increases with confining pressure. The peak is much more prominent at lower pressures, becoming less distinguishable at 12 MPa. There is a transition from brittle to ductile behaviour, with the effects of cementation being suppressed by increasing confinement. The dilation decreases with increasing confining pressure.

The flexibility of the membrane is demonstrated by observing the failure modes after deformation. Figure 9 shows photographs of cemented specimens after shearing at 1 and 12 MPa confining pressure, revealing shear planes at 1 MPa and barrelling at 12 MPa. This contrast in behaviour in the numerical samples is best observed by plotting particle rotations. Figure 10 shows the particle rotations on a vertical plane at 1 and 12 MPa confining pressures, at the point of maximum rate of dilation (1·0 and 7·5% axial strain, respectively). No clear shear plane is visible at 12 MPa, whilst there is a prominent shear plane visible at 1 MPa. The samples sheared at higher pressures display the correct barrelling failure and there is transitional behaviour in between these pressures. Without a flexible membrane, the formation of these failure modes would be inhibited, as shown by Cheung & O'Sullivan (2008).

CONCLUSIONS

A DEM model has been created that successfully simulates high-pressure triaxial tests on cemented and uncemented sand, with a flexible membrane allowing the correct deformation to develop. The model presented features a simple and effective way to apply the correct confining pressure after the sample becomes distorted and the membrane exhibits a non-uniform shape. The flexible boundaries also allow the vertical component of confining pressure to be applied to the specimen.

Simulations highlighting the ability to accommodate various failure modes have been performed. The correct qualitative behaviour for cemented sand has been observed with regard to varying confining pressure. The correct transition from brittle to ductile behaviour was witnessed with increasing confining pressure, with high pressures suppressing the effects of cementation. The flexible membrane permits a well-defined peak strength, dilation and formation of a shear band at low confining pressures, with a less well-defined peak and more volumetric contraction and no visible rupture plane at high confining pressures. Without a flexible membrane, the formation of these failure modes would be inhibited, as shown in previous literature. The method presented here shows much promise for the future modelling of triaxial tests using the DEM.

REFERENCES

Asghari, E., Toll, D. & Haeri, S. (2003). Triaxial behaviour of a cemented gravelly sand. *Geotech. Geol. Engng* **21**, No. 1, 1–28.

Belheine, N., Plassiard, J., Donze, F., Darve, F. & Seridi, A. (2009). Numerical simulation of drained triaxial test using 3D discrete element modelling. *Comput. Geotech.* **36**, No. 1, 320–331.

Cheung, G. & O'Sullivan, C. (2008). Effective simulation of flexible lateral boundaries in two and three-dimensional DEM simulations. *Particuology* **6**, No. 6, 483–500.

Coop, M. & Atkinson, J. (1993). The mechanics of cemented carbonate sands. *Géotechnique* **43**, No. 1, 53–68.

Haeri, S., Hamidi, A. & Tabatabaee, N. (2004). The effect of gypsum cementation on the mechanical behaviour of gravely sands. *Geotech. Test. J.* **28**, No. 2, 335–360.

Henkel, D. J. & Gilbert, G. D. (1952). The effect of the rubber membrane on the measured compression strength of clay samples. *Géotechnique* **3**, No. 1, 20–29.

Itasca (2005). *Particle flow code in three dimensions, software manual*. Minneapolis, MN: Itasca Consulting Group Inc.

Iwashita, K. & Oda, M. (1998). Rolling resistance at contacts in simulation of shear band developments by DEM. *J. Engng Mech.* **124**, No. 3, 285–292.

Marri, A., Wanatowski, D. & Yu, H. (2012). Drained behaviour of cemented sand in high pressure triaxial compression test. *Geomech. Geoengng*, http://dx.doi.org/10.1080/17486025.2012.663938.

O'Sullivan, C. & Cui, L. (2009). Micromechanics of granular material response during load reversals: combined DEM and experimental study. *Powder Technol.* **193**, No. 3, 289–302.

Potyondy, D. & Cundall, P. (2004). A bonded-particle model for rock. *Int. J. Rock Mech. Mining Sci.* **41**, No. 8, 1329–1364.

Salot, C., Gotteland, P. & Villard, P. (2009). Influence of relative density on granular materials behaviour: DEM simulations of triaxial tests. *Gran. Matter* **11**, No. 4, 221–236.

Schnaid, F., Prietto, P. & Consoli, N. (2001). Characterization of cemented sand in triaxial compression. *J. Geotech. Geoenviron. Engng* **127**, No. 10, 857–868.

Sitharam, T. G., Dinesh, S. V. & Shimizu, N. (2002). Micromechanical modelling of monotonic drained and undrained shear behaviour of granular media using three-dimensional DEM. *Int. J. Numer. Anal. Methods Geomech.* **26**, No. 12, 1167–1189.

Utili, S. & Nova, R. (2008). DEM analysis of bonded granular geomaterials. *Int. J. Numer. Anal. Methods Geomech.* **32**, No. 17, 1997–2031.

Wang, Y. & Leung, S. (2008). A particulate-scale investigation of cemented sand behaviour. *Can. Geotech. J.* **45**, No. 1, 29–44.

Wang, Y. & Tonon, F. (2009). Modelling triaxial test on intact rock using DEM with membrane boundary. *J. Engng Mech.* **135**, No. 9, 1029–1037.